nature communications

Article

https://doi.org/10.1038/s41467-025-57418-0

Operando TEM study of a working copper catalyst during ethylene oxidation

Received: 27 July 2024

Accepted: 19 February 2025

Published online: 27 February 2025

Check for updates

Wenqian Yu[1,2,7], Shengnan Yue[1,2,7], Minghe Yang[1,2], Masahiro Hashimoto[3], Panpan Liu[1,2], Li Zhu[1,2], Wangjing Xie[1,2], Travis Jones[4] ✉, Marc Willinger[5,6] ✉ & Xing Huang[1,2,6] ✉

Active catalysts are typically metastable, and their surface state depends on the gas-phase chemical potential and reaction kinetics. To gain relevant insights into structure-performance relationships, it is essential to investigate catalysts under their operational conditions. Here, we use *operando* TEM combining real-time observations with online mass spectrometry (MS) to study a Cu catalyst during ethylene oxidation. We identify three distinct regimes characterized by varying structures and states that show different selectivities with temperature, and elucidate the reaction pathways with the aid of theoretical calculations. Our findings reveal that quasi-static Cu_2O at low temperatures is selective towards ethylene oxide (EO) and acetaldehyde (AcH) via an oxometallacycle (OMC) pathway. In the dynamic Cu^0/Cu_2O oscillation regime at medium temperatures, partially reduced and strained oxides decrease the activation energies associated with partial oxidation. At high temperatures, the catalyst is predominantly Cu^0, partially covered by a monolayer Cu_2O. While Cu^0 is extremely efficient in dehydrogenation and eventual combustion, the monolayer oxide favors direct EO formation. These results challenge conclusions drawn from ultra-high vacuum studies that suggested metallic copper would be a selective epoxidation catalyst and highlight the need for *operando* study under realistic conditions.

Electron microscopy has played a significant role in advancing our understanding of catalysis[1,2]. It guides the optimization of synthesis protocols, delivers information about structure-performance relations, particle-support interactions and reaction-induced modifications that eventually lead to catalyst deactivation[3,4]. Modern analytical electron microscopes can reveal structural details at sub-Ångstrom resolution and deliver information about the composition and chemical state of atomic arrangements[5,6]. However, due to the strongly interacting nature of electrons, conventional electron microscopes require a good vacuum along the optical path of the beam to delivers detailed information about a thermodynamic equilibrium state. This state is, however, likely not an accurate representative of the active phase. In view of the quest to uncover the nature of active structures/sites, imaging must be done during operation.

Since the early attempts of Ernst Ruska in 1942[7], the instrumentation for in situ transmission electron microscopy (TEM) has undergone significant development and improvement[8–11]. In situ TEM now allows for the study of gas-solid interactions, providing atomic-scale insights into adsorbate-induced structural and chemical changes[12–24]. For example, the pioneering work of Hansen et al. on copper nanoparticles has revealed the shape change of zinc oxide-supported copper nanoparticles in response to changes in the

[1]College of Chemistry, Fuzhou University, Fuzhou, China. [2]Qingyuan Innovation Laboratory, Quanzhou, China. [3]JEOL (EUROPE) SAS, allée de Giverny, Croissy-sur-Seine, France. [4]Theoretical Division, Los Alamos National Laboratory, Los Alamos, NM, USA. [5]Department of Chemistry, Technical University of Munich, Garching, Germany. [6]Scientific Center for Optical and Electron Microscopy, ETH Zurich, Zurich, Switzerland. [7]These authors contributed equally: Wenqian Yu, Shengnan Yue. ✉e-mail: tejones@lanl.gov; marc.willinger@tum.de; xinghuang@fzu.edu.cn

surrounding atmospheres (H_2, H_2/H_2O, and H_2/CO) at low pressures[25]. More recently, the use of sealed MEMS chips enabled in situ TEM at elevated pressure in combination with on-line mass spectrometry and thus, simultaneous imaging and detection of catalytic conversion, and thus, the realization of *operando* experiments that provide unparalleled insights into the structure-performance relationships under working conditions[17,23,26,27]. Our recent in situ TEM study on titania-supported platinum particles has revealed that the often-described encapsulated state of this prototype strong metal-support interaction (SMSI) system[28] is lost when switching from a reducing or oxidizing atmosphere to a reactive redox atmosphere (O_2 to H_2/O_2 mixture)[14].

Building on earlier in situ electron microscopic studies on the redox behavior of Cu under specific gases (H_2, CO, or O_2) and model catalytic reactions[13,19,29–32], this work is focused on investigating the state evolution and dynamics of Cu in more complex partial oxidation reactions, i.e., the ethylene (partial) oxidation by *operando* TEM. The choice of this catalytic system is motivated by the fact that Cu can be added to Ag-based catalysts to improve the selectivity in ethylene epoxidation[11]. Moreover, Cu oxides alone have been shown to be active in ethylene epoxidation, while metallic Cu has been found to have a high selectivity in higher olefin epoxidation[33–35]. For example, UHV studies of styrene partial oxidation show the Cu(111) surface is 100 % selective to the epoxide[33]. The remarkable selectivity of metallic Cu has been explained by its strong oxygen bonding and relatively weak carbon bonding, favoring the path to epoxide formation through an oxametallacycle (OMC) intermediate[36]. Nonetheless, due to its high oxygen affinity, Cu is prone to oxidation under typical epoxidation conditions, resulting in the formation of bulk oxides. Greiner et al. examined the selectivity of CuO and Cu_2O under ethylene epoxidation conditions and found that both oxide phases exhibited low epoxide selectivity[37]. Interestingly, they also found that adjusting the conditions to a low O_2 chemical potential could maintain a metastable state close to the phase transition from Cu_2O to CuO, giving rise to a 20-fold increase in selectivity compared to conditions far from the phase transition. The enhanced selectivity was attributed to the presence of metastable adsorbed oxygen species on Cu_2O at the onset of the Cu_2O to CuO phase transition. Such phenomenon has been observed not only in Cu but also in Pd and other transition metals[13,17,38,39], where enhanced reactivity is associated with metastable states at phase boundaries[40,41].

While the CuO-Cu_2O phase transition and its influence on selectivity has been investigated[37], the effects of the phase transition between Cu_2O and Cu, and the coexistence of metal and oxide, on catalytic performance have not been well studied. This is particularly important as metallic Cu has demonstrated high selectivity in catalyzing olefin epoxidation under UHV conditions[33]. Additionally, the phase transition between Cu_2O and Cu can lead to the generation of adsorbed O_2 species[13], which are thought to play a crucial role in enhancing selectivity[36,42]. In this work, we conduct *operando* TEM that combines real-time imaging with online MS analysis to investigate the structures of a working Cu particle catalyst during an O_2-diluted ethylene oxidation reaction. A broad temperature range (from 200 to 950 °C) is chosen for investigation in order to fully explore the various possible states/structures of Cu and their correlations with catalytic reactivity. By adjusting the chemical potential of O_2, we are able to study a regime in which Cu and Cu_2O coexist within a specific temperature range. Beyond that, in a high-temperature regime where the bulk metallic phase is kinetically accessible due to the rapid reduction of the oxide by ethylene, we observe total oxidation, i.e., the production of CO_2 and water. Additionally, in a low-temperature regime where Cu_2O alone is present, the catalyst favors selective products, *i.e.*, AcH and EO.

Results

Morphological evolution

The initial Cu NPs with sizes in the range of 25 to 200 nm (Fig. S1) were treated in a H_2/O_2 mixture at 500 °C using a gas-flow TEM holder (Fig. S2). As we reported earlier[13], it is possible to adjust the average particle size through leverage between particle splitting, which mostly affects larger partially oxidized particles during swift reduction processes, and sintering of smaller reduced particles in a redox atmosphere. Following this redox treatment that resulted in particles ranging mainly from 10 nm to 100 nm (Fig. S3), the temperature was dropped to 200 °C. Subsequently, H_2 was removed from the gas-flow and replaced by a constant flow of C_2H_4 to set oxygen-lean C_2H_4 oxidation conditions (C_2H_4:O_2 = 40:1).

In situ observation at 200 °C shows that the particles exhibited a hollow structure (Figure S4), which is induced by the Kirkendall effect[43,44] due to surface oxidation and Cu outward diffusion during cooling after the initial redox treatment in H_2/O_2 mixture at 500 °C. To study how the shape, size, and dynamic behavior of Cu particles depends on temperature under conditions of C_2H_4 oxidation, we conducted in situ observation across a broad temperature range from 200 to 900 °C (Fig. 1). We found that at a temperature range between 200 °C and 300 °C, the hollow structure remains stable with only minimal changes observed (Fig. 1a_1 and a_2). However, once the temperature is raised to 400 °C and 500 °C, the hollow structures collapse (Fig. 1a_3 and a_4), which is indicative for partial reduction of the Cu particles and thus, activation of C_2H_4. Holding the temperature at 500 °C for a few minutes does not result in any further significant changes in the overall shape of NPs (Fig. S5). Once the temperature is increased to 600 °C, some of the larger Cu particles start to show dynamic behavior (Fig. 1b, Supplementary Movie S1), including particle reshaping and migration on the silicon nitride support (i.e., the window of the MEMS chip). Substantial increase in particle dynamics due to particle fragmentation and morphological transformation into a head-tail structure is observed when the temperature is increased further from 600 °C to 700 °C. At 700 °C, the particles start to behave highly dynamic, with particle splitting, sintering, migration, and reshaping (Fig. 1c, Supplementary Movie S2). The observed redox dynamics are reminiscent of the earlier reported behavior of Cu under hydrogen oxidation reaction[13,45]. Further increasing the temperature to 800 °C results in sintering and simultaneously, a morphological change from elongated to spherical shapes (Fig. 1d, Supplementary Movie S3). While dynamic behavior persists at 800 °C, it is less pronounced compared to that at 700 °C. Additionally, it is noted that as the temperature increases, the roughness of the SiN membrane support also increases. This rise in surface roughness is correlated with the increased instability of the support at higher temperatures and the formation of carbonaceous materials resulting from the decomposition of C_2H_4. Particularly in the latter case, some smaller particles get trapped within the framework of the carbonaceous materials, thereby restricting their mobility (Supplementary Movie S4). Moreover, some of these particles may be contaminated by carbon species, resulting in deactivation. When the temperature is finally increased to 900 and 950 °C (Fig. 1e and f, Supplementary Movies S5 and S6), the particle dynamics are strongly inhibited, with most particles remaining static or undergoing only stationary surface reconstruction. Additionally, the sizes of particles increase due to sintering (Fig. 1c–f).

Phase analysis by in situ electron diffraction

To gain insights into the structure and phase composition of particles at different temperatures, in situ selected-area electron diffraction (SAED) was conducted (Fig. 2a–f). The line profiles derived from the electron diffraction patterns are shown in the right panels of Fig. 2g–l. Analysis of the diffraction data reveals that in the temperature range of 300 to 500 °C, the particles exhibit a Cu_2O phase (Fig. 2a, b and g, h). The *d*-spacing of Cu(111) (2.09 Å) is very similar to that of Cu_2O (2.13 Å),

https://doi.org/10.1038/s41467-025-57418-0

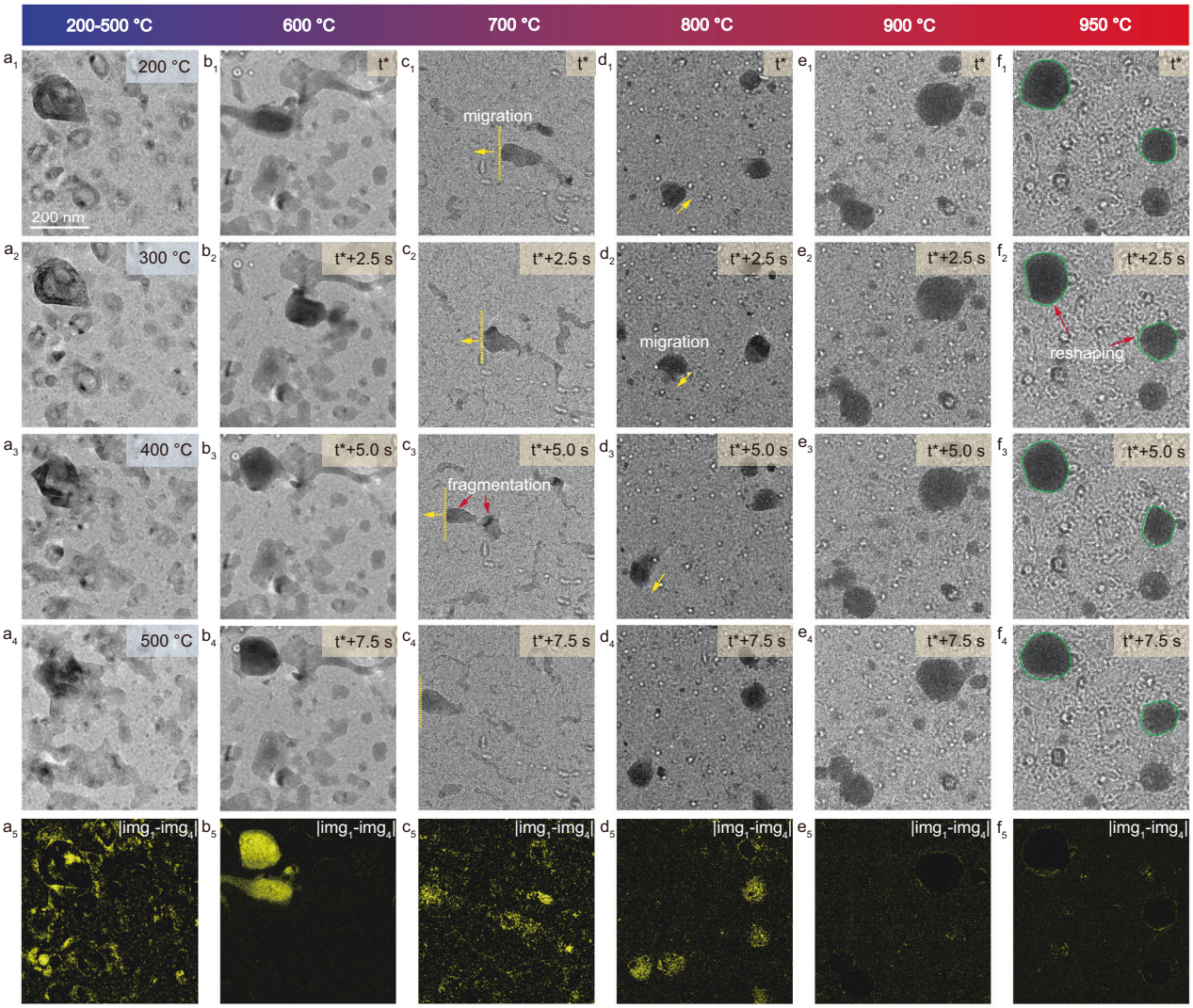

Fig. 1 | Morphological evolution. (a_1-a_4, b_1-b_4, c_1-c_4, d_1-d_4, e_1-e_4, f_1-f_4) In situ TEM observations at different temperatures (total pressure: 708 mbar; p_{O2} = 4.27 mbar, p_{C2H4} = 170.6 mbar). (a_5, b_5, c_5, d_5, e_5, f_5) Difference between image 1 and image 4.

causing an overlap of the respective peaks when both phases are present. This can be observed in the intensity profile at 600 °C, where the Cu_2O(200) peak is slightly shifted to a higher value of 1/nm (Fig. 2c, i), indicating the presence of a minor portion of Cu(111). This shift is more obvious in the intensity profile recorded at 700 °C (Fig. 2d, j). Furthermore, the Cu(200) peak is present, confirming the coexistence of Cu and Cu_2O at 700 °C. In situ observation at 700 °C shows that the diffraction spots (attributed to Cu and Cu_2O phases) change over time (Supplementary Movie S7), corroborating structural dynamics and interconversion at the Cu/Cu_2O phase boundary. A similar phase coexistence is observed at 800 °C (Fig. 2e and k, Supplementary Movie S8), although the portion of the Cu_2O phase has decreased significantly compared to that at 700 °C, as evidenced by the reduced intensity of the Cu_2O(111) peak. At 900 °C (and 950 °C, see Figure S6), the Cu_2O phase diminishes, leading to the predominance of the metallic Cu phase (Fig. 2f, l).

Overall, real-time observations unveil that the particle size, shape, and phase composition are strongly depending on the chemical potential of the gas phase. Within the temperature range of 600 °C to 800 °C, the particles exhibit dynamic behavior characterized by oscillatory phase transitions between Cu and Cu_2O, whereas below 600 °C and 800 °C, the particles primarily exist respectively as Cu_2O and Cu, a decrease in the level of or even a complete cessation of structural dynamics are observed.

Structure-performance relationships

Following the identification of three distinct states of the Cu catalyst at different temperature ranges, we performed further *operando* TEM, which combined in situ high-resolution observations with on-line MS to explore atomic-level structures and the correlations between structures and catalytic reactivity (Fig. 3a). At 400 °C, TEM and HRTEM images show only the Cu_2O phase (Fig. 3b, c), consistent with in situ electron diffraction results. In contrast, at 700 °C, HRTEM images reveal both Cu^0 and Cu_2O phases within dynamic particles, where each particle has a metallic head connected to a Cu_2O tail (Fig. 3d, e, Figure S7, and Supplementary Movie S9). The volumes of the head and tail change oppositely due to an oscillatory phase transition, with the metallic portion increasing at the expense of the Cu_2O portion during the reducing half-cycle, and vice versa during re-oxidation – however, neither reduction nor oxidation complete. The different lattice constant between Cu^0 and Cu_2O results in interfacial strain. Structural analysis reveals that the lattice *d*-spacing of Cu_2O(111) is constrained by 1.3% at the Cu/Cu_2O interface compared to the region away from the interface (Fig. 3e, f). Moreover, due to the constant oscillatory phase

https://doi.org/10.1038/s41467-025-57418-0

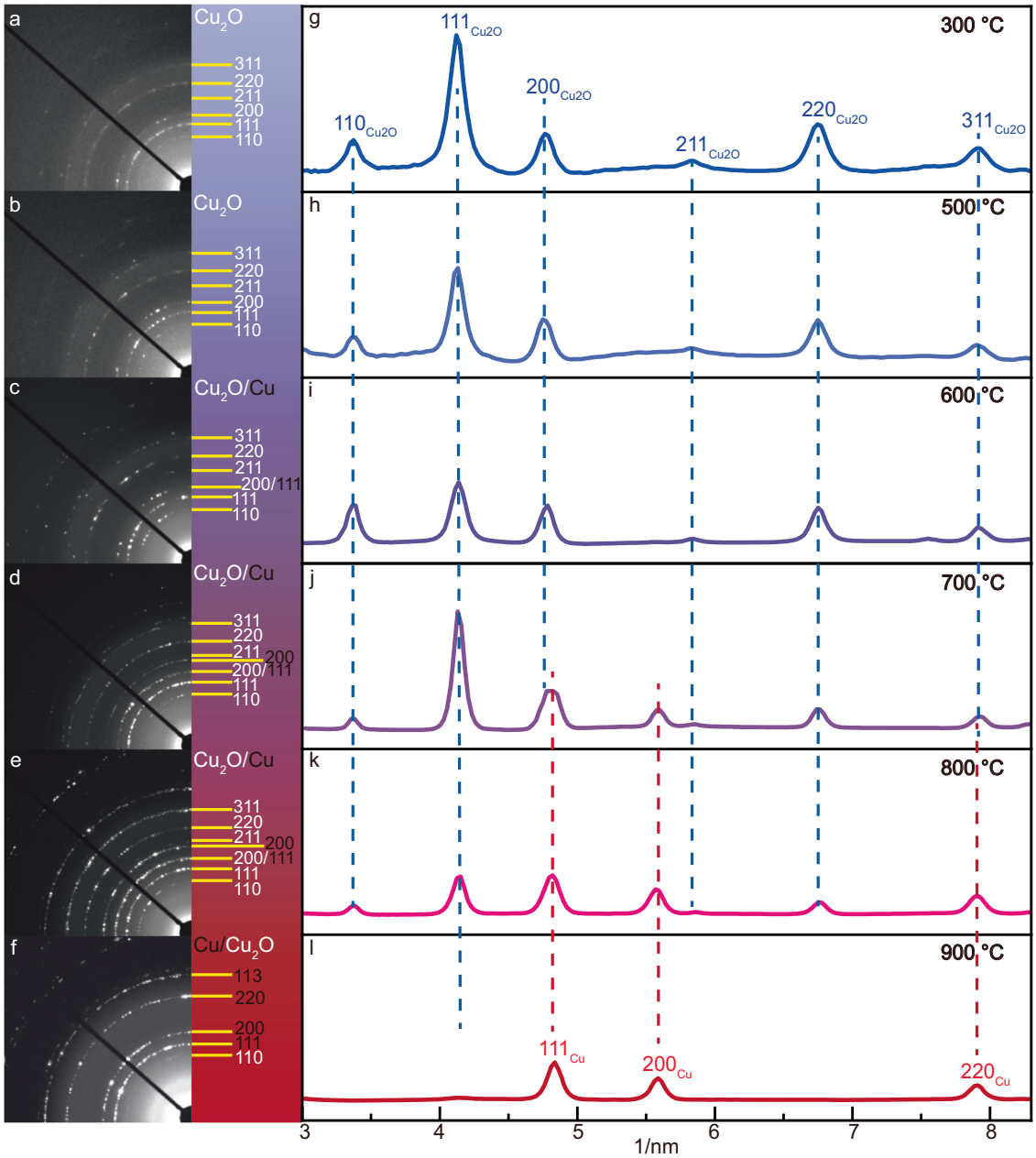

Fig. 2 | Phase analysis based on in situ SAED. a–f In situ recorded SAED patterns and (**g–l**) azimuthal average (100 frames, 10 s) and time-integrated 2D diffraction patterns of Cu particles recorded at different temperatures in the gas mixture of C_2H_4, O_2 and He (total pressure: 708 mbar; p_{O2} = 4.27 mbar, p_{C2H4} = 170.6 mbar).

transitions between Cu^0 and Cu_2O, partially reduced Cu_2O (with oxygen vacancies), may transiently exist. This hypothesis is further strengthened by the detection of partially reduced PdO via in situ XPS during oscillatory phase transitions between Pd^0 and PdO in our previous study, albeit in a different system[17]. Finally, at 900 °C, the particles exhibit a *quasi*-static state with metallic Cu decorated by a monolayer of Cu_2O (Fig. 3g, h). However, the corners and some specific facets of particles are not fully covered and reveal Cu metallic surfaces (Fig. 3h), demonstrating that both Cu^0 and Cu_2O monolayer expose to the gas atmosphere at 900 °C. A similar thin oxide surface layer, along with partially exposed metallic Cu, was also observed on Cu particles during hydrogen oxidation at high temperatures[13].

The online MS analysis clearly shows a rise in oxygen consumption and water formation as the temperature is increased from 400 to 950 °C (Fig. 3i). More importantly, it detects the mass signals of 44 and 43 *m/z*, which are associated with CO_2, EO, and AcH. Thus, in situ MS data ambitiously confirm that the catalyst is active in the partial oxidation of C_2H_4. Typically, this reaction can yield selective oxidation products (EO and AcH), along with the full oxidation product, CO_2. Since these chemicals share the same atomic weight of 44 amu, they would all contribute to a mass signal of 44 *m/z* in the mass spectrum if present. Acetaldehyde and ethylene oxide could additionally generate a mass signal at 43 *m/z*, which can be used to verify their presence[46]. However, due to their identical mass and fragments, AcH and EO cannot be differentiated by MS[42].

If we hypothesize that the mass 43 is solely attributed to the EO, we can estimate the relative generation rate of CO_2 (after deducting the contribution of ethylene oxide from the mass 44 signal) with temperature, and provide qualitative insights into the selectivity towards partial or full oxidation products (Fig. 3j, Table S1). In short, our result suggests that in the temperature range between RT and 500 °C, where the catalyst is Cu_2O and no structural dynamics (due to

https://doi.org/10.1038/s41467-025-57418-0

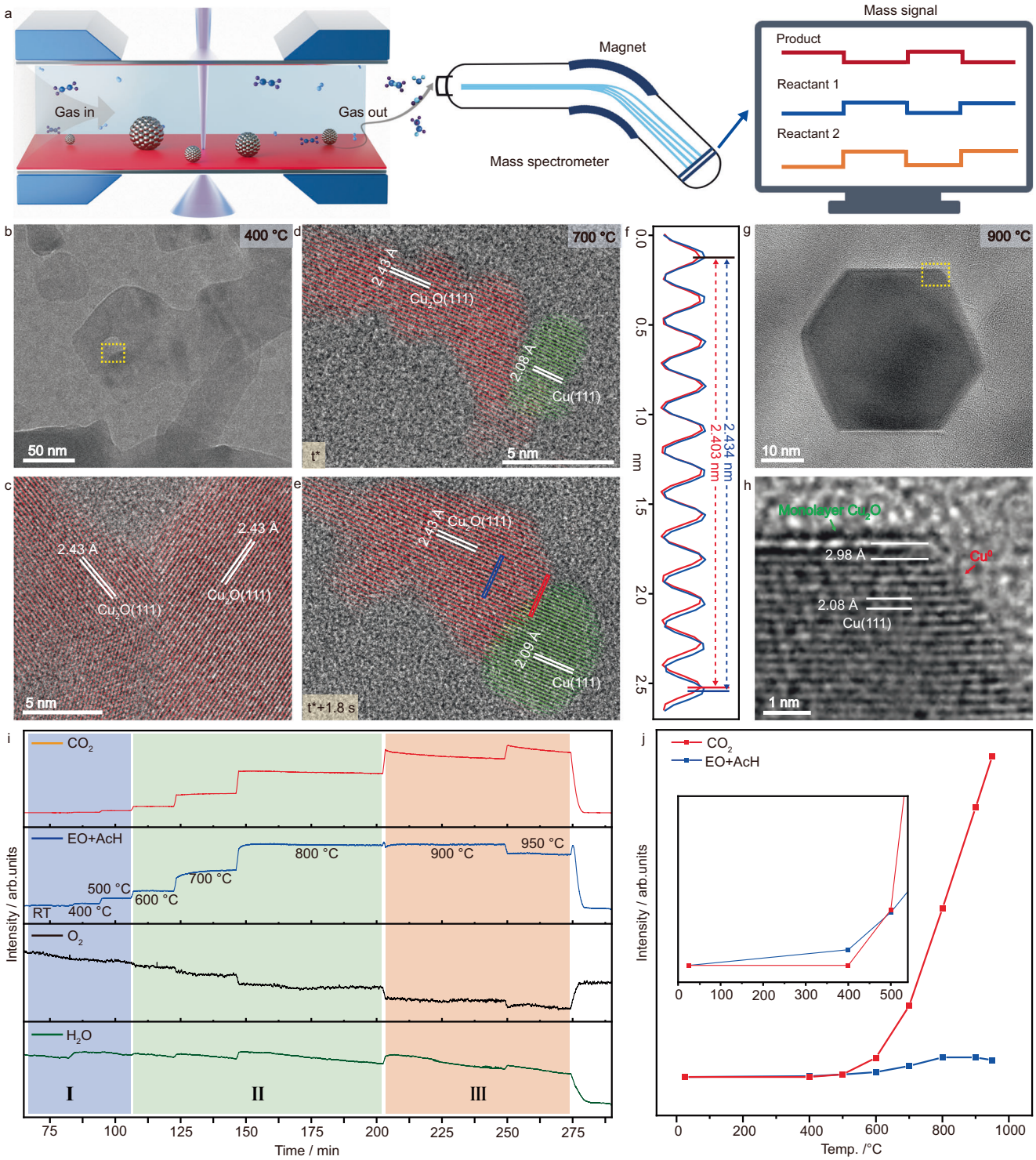

Fig. 3 | Structure-performance relationships. (**a**) Schematic illustration of *operando* TEM technique. (**b**–**e**, **g**, **h**) In situ HRTEM observations and (**i**, **j**) online MS study of Cu catalysts at different temperatures under conditions of the O_2-diluted C_2H_4 oxidation reaction (total pressure: 708 mbar; p_{O2} = 4.27 mbar, p_{C2H4} = 170.6 mbar). **f** Lattice distance profiles for Cu_2O measured at the Cu/Cu_2O interface and in the central region of the Cu_2O portion.

an oscillatory phase transition) are present, the selective oxidation products are dominant (inset of Fig. 3j). In contrast, in the temperature range of 600 to 800 °C, where the catalyst undergoes oscillatory phase transitions between Cu and Cu_2O, there is a significant increase in CO_2 formation rate, indicating a shift towards the dominance of full oxidation (Fig. 3i). As the temperature exceeds 900 °C, metallic Cu (with a mono-layer of Cu_2O) becomes the main phase and the oscillatory phase transition was suppressed. In such a state, the formation of selective oxidation products drops, while the one of full oxidation products further increases. A similar picture is obtained when assuming that the mass signal of 43 *m*/*z* originates solely from acetaldehyde (refer to Fig. S8 and Table S2 for more details). It should be mentioned that EO and AcH are unstable under the applied high-temperature reaction conditions and would be decomposed[47–49],

https://doi.org/10.1038/s41467-025-57418-0

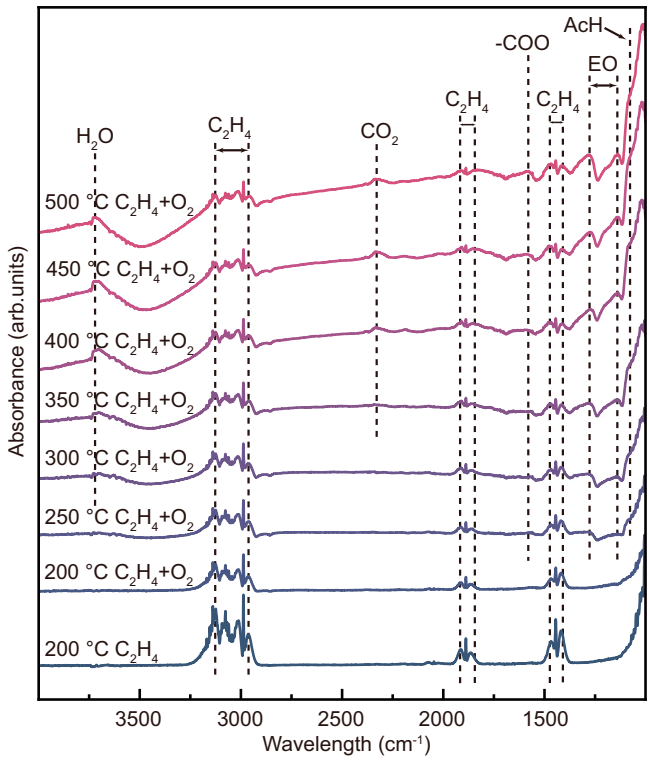

Fig. 4 | Investigation of reaction intermediates/products. In situ DRIFTS spectra were recorded from Cu NPs in pure C_2H_4 and a mixture of C_2H_4 and O_2 at elevated temperatures.

which can lead to a reduction in intensity of 43 *m/z*. Overall, the combination of in situ observations with on-line MS reveals three distinct regimes. They show different selectivity towards partial- and full oxidation, coinciding with three different states of catalysts.

In situ diffuse reflectance infrared Fourier-transformed spectroscopy (DRIFTS) study

In situ DRIFTS measurements were carried out to gain a further understanding of the ethylene oxidation process on Cu particles (Fig. 4). To overcome the possible low signal due to the dark color of copper powder, SiO_2 was added and mixed with the copper powder to create a grayish brown color. The in situ DRIFTS experiment involved introducing ethylene into the reaction cell at 200 °C for 45 minutes, followed by the addition of oxygen at the same temperature for another 45 minutes. The temperature was then incrementally raised to 500 °C in 50 °C intervals, with each temperature being maintained for 45 minutes. The in situ DRIFTS spectrum obtained at 200 °C under pure ethylene gas reveals the presence of multiple vibration bands of gas-phase C_2H_4 at 3150–2900 cm^{-1} (ν9, ν11, ν2 + ν12), 1900-1800 cm^{-1} (ν7 + ν8), 1500–1400 cm^{-1} (ν12), and 1006 cm^{-1} (ν7)[50], respectively. Upon the introduction of oxygen at 200 °C, the intensities of these bands decrease, primarily due to a reduction in partial pressure. With increasing temperature to 250 °C, two weak bands emerge at 1282 cm^{-1} and 1101 cm^{-1}, corresponding to C-O-C stretching vibration and C-O stretching vibration of EO, respectively[51]. Moreover, a band at 1080 cm^{-1} appear, which can be assigned to AcH, formed probably from the EO isomerization[51]. Simultaneously, the bands originating from gas-phase C_2H_4 weaken, indicating the occurrence of the epoxidation reaction at this temperature. It is important to note that no signals from water or CO_2 (2330 cm^{-1}, O=C=O symmetric stretching)[51,52] are detected, indicating that full oxidation was still hindered. Upon raising the temperature to 300 °C, a weak broad band near 3715 cm^{-1} appears, which can be assigned to O-H stretching vibration[53], suggesting water formation. Additionally, an absorption band at 1580 cm^{-1} attributed to the asymmetric stretching vibration of surface carboxylates is detected[52]. With the increase of temperature to 400 °C, the intensities of bands assigned to C_2H_4 decrease further, and simultaneously, the bands assigned to AcH and EO intensify. Interestingly to note that CO_2 signal is observed at this temperature, suggesting the onset of full oxidation. Further increasing the temperature to 500 °C leads to a slight decrease in intensity of the gas phase C_2H_4, due to further increase in conversion. Overall, in situ DRIFTS study reveals that at lower temperatures partial oxidation favors whereas at higher temperatures full oxidation gets enhanced, consistent with *operando* TEM results.

Theoretical simulations

To gain insight into the kinetics of ethylene (partial) oxidation under the conditions explored in this work, we performed density functional theory (DFT) calculations on a series of Cu_2O(110) surfaces at varying degrees of reduction and on metallic Cu(111) with varying degrees of in-plane strain. The oxide surface was modeled as the pristine oxide, which is representative of the low-temperature catalyst. We then explored the role of surface reduction by sequentially removing subsurface oxygen to represent the catalyst at higher temperatures. To capture the behavior present at the highest temperatures, Cu_2O(110) surfaces were modeled with 1–5% compressive strain to capture the effects of the interfacial strain between Cu_2O/Cu observed in TEM. For both the metal and the oxide we explored the well-known OMC mechanism[37,54–56]. On the metallic surface, we also explored dehydrogenation of the OMC, which results in combustion[57]. On the oxide, a direct path to EO was also considered[55].

At low temperatures where the oxide is observed in TEM, we find that both EO and AcH can be produced through the OMC mechanism on the defect-free surface (Fig. 5), with activation energy (E_a) of 0.6 eV (state 4 in the figure) for OMC formation compared to 1.9 eV for direct EO formation (state 2 in the figure). Once the OMC forms (state 5 in the figure), decomposition into AcH has a lower E_a (1.0 eV) via state 8 in the figure than into EO (1.5 eV) via state 6 in the figure. This result suggests the pristine oxide will produce a significant fraction of AcH, which will contribute to the $m/z = 43$ signal[42] as AcH is not immediately burned on Cu_2O. At higher temperatures, the oxide begins to be reduced through the consumption of oxygen on the active surface, which strongly impacts the reaction kinetics in complex ways.

As the Cu_2O surface is reduced, the activation energy for direct EO formation drops from 1.9 eV to 1.0 eV. This is shown by way of states 2′ and 2″ in Fig. 5. State 2′ shows the activation energy for direct EO formation from on the Cu_2O surface with 1/8 ML adsorbed oxygen. State 2″ shows the activation energy for direct EO formation from on the Cu_2O surface with 1/8 ML adsorbed oxygen but no subsurface oxygen. In comparison to the direct EO pathway, the apparent activation energy for both AcH and EO increases on the reduced surface. From Fig. 5, the apparent activation energy for AcH (EO) formation on the pristine oxide can be seen to be 1.4 eV (1.9 eV). While not shown, the apparent activation energy for AcH (EO) formation on the Cu_2O surface with 1/8 ML adsorbed oxygen is 1.8 eV (1.5 eV), and on the surface without subsurface oxygen the apparent activation energies are 1.6 eV (1.8 eV), respectively. The metal/oxide interface shows similar, albeit slightly higher, barriers for partial oxidation (Fig. S9). These results suggest that the oxide surface can remain active in the production of partial oxidation products even as it becomes non-stochiometric and with the appearance of metal/oxide interfaces. Notably, the activity of direct EO formation increases with (sub)surface reduction, potentially making the non-stochiometric/partially reduced oxide more selective in EO production than the pristine oxide or the metal/oxide interface.

The increase in activity of the Cu_2O surface with reduction will result in the autocatalytic formation of metallic copper through a

https://doi.org/10.1038/s41467-025-57418-0

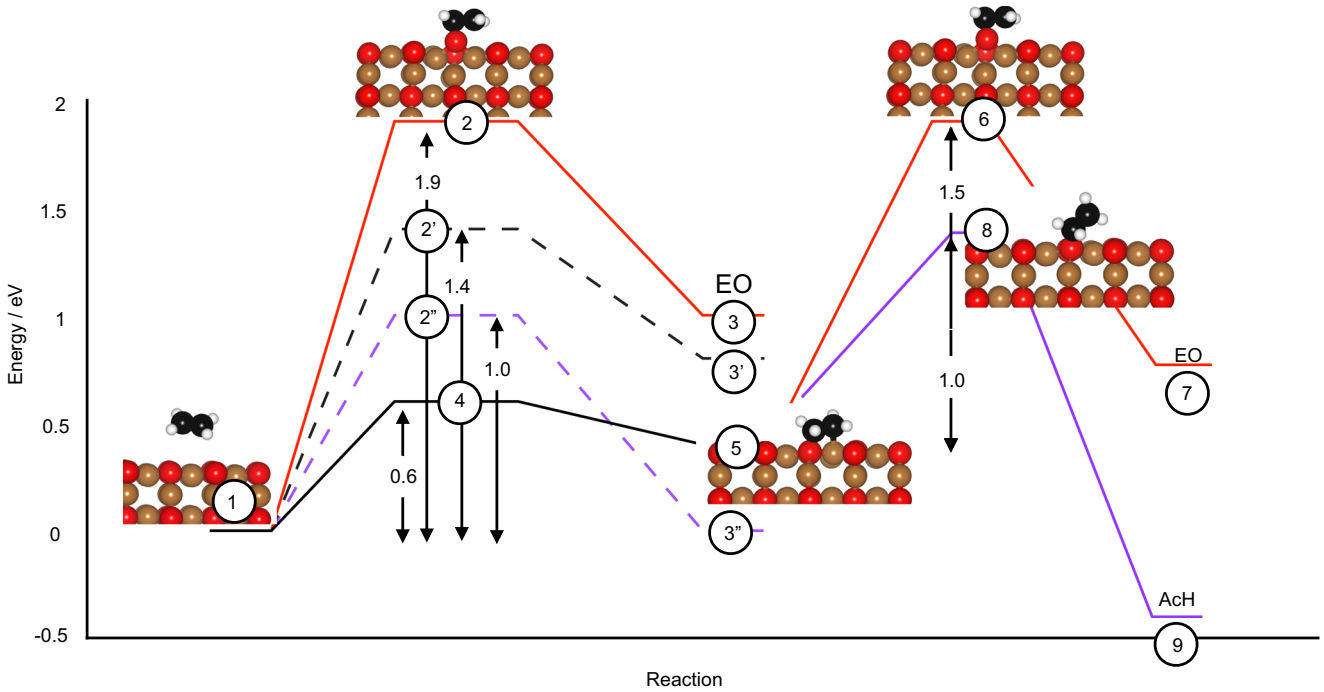

Fig. 5 | Computed ethylene (partial) oxidation pathways. State 1 corresponds to adsorbed ethylene. State 2 is the direct transition state to EO on the pristine surface. State 2′ is the direct transition state to EO on the surface with 1/8 ML surface oxygen. State 2″ is the direct transition state to EO on the surface 1/8 ML surface oxygen but no subsurface oxygen. States 3, 3′, and 3″ are the corresponding EO products. State 4 is the transition state to an OMC (only shown for the pristine surface). State 5 is the OMC. State 6 is the transition state from the OMC to EO; state 7 is the product EO. State 8 is the transition state from the OMC to AcH; state 9 is the product AcH.

purely kinetic process; note the oxide is thermodynamically stable under all oxygen chemical potentials used in this work[58]. Above 700 °C, SAED shows metallic Cu forms through such an autocatalytic process (Fig. 2d, j). Under these conditions the coexistence of metallic and oxide phases results in interfacial strain in the oxide at the oxide/metal interface. This strain slightly perturbs the computed activation energies to EO and AcH from the OMC on the oxide (see Fig. S10); the former drops to 1.2 eV and the latter stays constant at 1.0 eV at 5% compressive strain. While the activation energy for OMC formation remains unchanged, the alterations in E_a are predicted to make the strained oxide at the metal/oxide interface more selective towards EO than the unstrained Cu_2O surface; the strained surface is also predicted to be more active than the unstrained oxide.

At higher temperatures, TEM shows metallic copper will eventually predominate. Moreover, TEM reveals the presence of a surface oxide on the metallic catalyst surface. The pathway for ethylene partial oxidation on such a surface oxide, modeled as a single layer of $Cu_2O(110)$ on metallic Cu, is shown in Fig. 6. As before, the OMC pathway is favored; direct EO formation (Fig. S11) is activated by 1.2 eV as compared to the competing OMC formation that is activated by 0.7 eV. Inspection of the figure shows that once the OMC forms, it selectively decomposes into EO by crossing a barrier of 0.9 eV compared to 1.2 eV for AcH formation and 1.9 eV for 2-oxoethyl formation (Fig. S12). Unlike the bulk oxide, this would make the single oxide layer selective in EO formation through the OMC pathway, though gas phase reactions will still cause EO decomposition at these high temperatures. We also considered the metallic surface (Fig. S13), which is characterized by similar E_a's as on the oxide surface. OMC formation has an E_a of 0.6 eV, which can decompose into EO (AcH) with an E_a of 1.1 eV (1.3 eV) or undergo rapid dehydrogenation with an E_a of 0.6 eV. Unlike the reaction on the oxide surface, the formation of the OMC on the metal is strongly exothermic, leading to an apparent activation energy for ethylene (partial) oxidation of 0.6 eV via dehydrogenation. As noted above, the dehydrogenation pathway is expected to result in total oxidation products[57], thus high CO_2 production rates are predicted on the metallic phase observed to form at high temperatures.

DFT then shows that at low T Cu_2O is active in AcH/EO production. As the temperature increases and the oxide becomes increasingly reduced, the AcH:EO ratio is predicted to drop as the activation energy associated with the direct formation of EO drops. This increased activity of Cu_2O at higher temperatures will eventually lead to the autocatalytic reduction of Cu_2O to metallic Cu, despite the fact that Cu_2O is the thermodynamically favored phase under the oxygen chemical potentials used in this work[58]. The lower activation energies associated with ethylene oxidation on the metallic surface can then lead to runaway reduction and eventually phase oscillations where kinetics drives the catalyst to a reduced state and thermodynamics drives it back to Cu_2O. At high enough temperatures, the runaway reduction dominates and metallic copper is the principal phase. While gas phase chemistry cannot be ignored at these high temperatures[47–49], the transformation to metallic copper is predicted to result in high total oxidation activity due to OMC dehydrogenation, in line with the experimental observations.

Discussion

Redox active metal catalysts typically undergo oxidation and/or reduction under reaction conditions[17,42,59,60]. These redox processes enable metal catalysts to actively participate in catalytic cycles and play a crucial role in catalytic performance. Capturing and understanding the redox dynamics and structural evolution of metal catalysts during catalytic reactions are essential for elucidating structure-performance relationships and the underlying reaction mechanisms.

In this study, we carried out *operando* TEM to investigate the structure-performance relationships of a working Cu catalyst during ethylene partial and total oxidation at varied temperatures. Despite being the subject of intensive research for two decades, spatially

https://doi.org/10.1038/s41467-025-57418-0

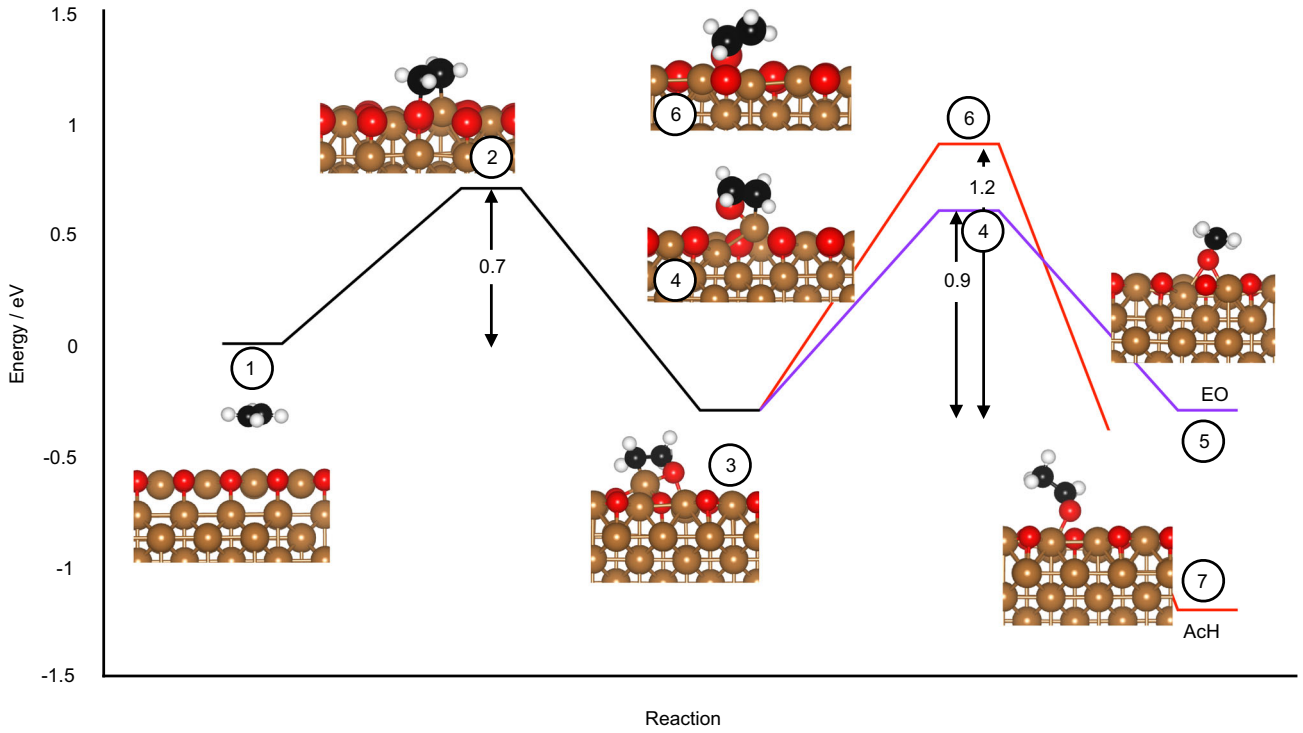

Fig. 6 | Computed ethylene (partial) oxidation pathways on a single layer of Cu_2O on Cu metal. State 1 shows adsorbed ethylene. State 3 is the OMC formed via state 2 with $E_a = 0.7$ eV. State 5 is EO formed via state 4 with $E_a = 0.9$ eV, and state 7 is AcH formed via state 6 with $E_a = 1.2$ eV.

resolved information regarding the catalyst state and dynamic structural changes of Cu catalysts, to the best of our knowledge, has remained unexplored. Inspired by previous UHV studies demonstrating the high selectivity of metallic copper surfaces in catalyzing styrene epoxidation[33], we conducted the experiments under an O_2-diluted condition to allow the formation of metallic Cu. However, the in situ results indicate that even at a high C_2H_4 to O_2 ratio of 40 to 1, the metallic phase is not detected between 200 °C and 500 °C, consistent with the findings by Greiner et al.[42]. Therefore, under industrial conditions with much higher O_2 chemical potential, the metallic surface/phase is likely absent.

In situ HRTEM and SAED analyses evidence that the catalyst has a Cu_2O phase in the temperature range of 200–500 °C. A morphological transition from hollow to solid NPs is observed with increasing temperature within this temperature range, indicating partial reduction of Cu_2O, likely due to enhanced activation of C_2H_4. Both online MS and in situ DRIFTS results demonstrate that the catalyst is active for partial oxidation of ethylene in this temperature window. DFT calculations suggest that both pristine Cu_2O and partially reduced Cu_2O are active in the selective oxidation of ethylene, with pristine Cu_2O favoring the OMC pathway for AcH/EO production, and reduced Cu_2O (oxygen vacancies in Cu_2O) favoring direct EO formation (Fig. 5 and Figure S10).

Rasing the temperature further to a range of 600–800 °C leads to a notable structural transformation from the relatively stable Cu_2O NPs to a highly dynamic state characterized by phase coexistence and oscillatory phase transitions between metallic Cu and Cu_2O. These oscillations resemble observations from our previous study on Cu during hydrogen oxidation (H_2:O_2 = 10:1, 400–600 °C). The phase transitions observed during ethylene (partial) oxidation, particularly the Cu_2O to Cu transition, suggest that lattice O participates in the catalytic process of the ethylene (partial) oxidation. The lattice O is replenished later via metal oxidation, where gaseous O_2 is converted into lattice O through dissociative adsorption. Such a redox cycle allows for the regeneration of active sites/phases that are crucial for the production of the selective products during the reaction[13,17,39]. In addition, phase oscillations lead to the formation of strained Cu_2O at the metal/oxide interface and non-stochiometric/partially reduced oxide, which are predicted to be more active and conductive for direct EO formation by our calculations. Phase oscillations also lead to the emergence of metallic Cu, which is shown to be favorable for CO_2 production, as shown in Fig. 6 and discussed in more detail in the next paragraph. Online MS data collected concurrently with in situ observations shows a substantial increase in signals for both selective products and full oxidation products (during increasing temperature from 600 to 800 °C), with the full oxidation products being dominant in this temperature regime. This finding indicates that the dynamic state of the catalyst (phase coexistence and oscillations) overall favors for the formation of full oxidation products.

When the catalyst is operated at 900 and 950 °C, the preference for full oxidation products is further amplified, leading to a decrease in the selectivity of partial oxidation products. At such high temperatures, the catalyst becomes less dynamic than it is at 600–800 °C. The resulting surface is characterized by a quasi-static state composed of Cu metal partially covered by a monolayer of Cu_2O, with the metal phase being predominant. The structure is again similar to that observed on Cu during hydrogen oxidation (H_2:O_2 = 10:1, 700–750 °C)[13], highlighting the existence of common structural features for Cu catalysts under redox reactions. The low epoxide selectivity under these conditions is at odds with previous UHV work on styrene epoxidation[33] and highlights the need to work under *operando* conditions and consideration of the chemical potential of the reactive environment. Our DFT simulations attribute the increased total oxidation to the high activity of the metal phase in promoting total oxidation via OMC dehydrogenation. The reduced partial oxidation activity can be linked to the diminished presence of the Cu_2O phase at higher temperatures. Although the single oxide layer is predicted to be active in EO formation through the OMC pathway, the oxidative decomposition of selective products via direct gas phase reaction at

high temperatures cannot be ruled out, which could lead to the consumption of these products and the generation of more CO_2[47–49].

Finally, we have proposed the rationale for the presence of phase coexistence and oscillatory phase transitions during the applied ethylene oxidation conditions based on DFT calculations. While Cu_2O is the thermodynamically stable phase, reaction kinetics drive the autocatalytic reduction of Cu_2O to Cu metal. Thermodynamics, however, pushes the metal back to Cu_2O via activating O_2, resulting in phase coexistence and oscillatory phase transitions. Indeed, a similar phenomenon has been reported in different catalytic systems, such as hydrogen oxidation on Cu and Ni[13,38,45], as well as methane oxidation on Pd[17,39], highlighting that the dynamic interplay between reaction kinetics and thermodynamics may play a common mechanism for the phase coexistence and oscillations in redox-active metals during redox reactions.

In summary, this study provides valuable insights into the structure-performance relationships of a Cu catalyst in an O_2-diluted ethylene partial oxidation reaction through a combined study of *operando* TEM, in situ DRIFTS, and DFT calculations. In particular, the dynamic visualization of the evolving active structures and their correspondingly varying catalytic functions with temperature underscores the importance of *operando* TEM in unveiling the dynamic nature and catalytically relevant structures and processes of catalysts, which are inaccessible through ex situ and *post mortem* characterizations. The findings of this study may also contribute to enhance our understanding of how phase coexistence and oscillations influence catalytic performance of redox-active metal catalysts in redox reactions.

Methods

Operando TEM

The Cu particles used in this work were purchased from Sigma Aldrich and were used as received. These Cu particles were dispersed in chloroform and then drop-casted onto a MEMS-based heating chip. Subsequently, the loaded chip was treated by O_2 plasma to remove organic residues and was followed by assembly into DENSsolutions gas-flow holder. The O_2 plasma was performed again on the assembled holder to remove the remaining organic residues. Afterward, the gas-flow holder was inserted into the chamber of an aberration-corrected GrandARM 300 F with the inlet tube connected to the DENSsolutions gas feeding system and the outlet connected to a quadrupole mass spectrometer (JEOL JMS-Q1500GC). After evacuating and flushing the gas-feeding system by He for 2 times, we added 20%H_2 and 2%O_2 (balanced with He) into the nanoreactor and increased the temperature to 500 °C (flow rate: 0.14 ml/min, pressure: 285 mbar) to refine the particle size via particle fragmentation. In the following, we decreased the temperature to 200 °C, removed H_2 and replaced it with C_2H_4 to settle the C_2H_4 oxidation condition (flow rate: 0.35 ml/min, total pressure: 708 mbar; $p_{O2} = 4.27$ mbar, $p_{C2H4} = 170.6$ mbar). The temperature was increased stepwise to 900 °C with 100 intervals and finally to 950 °C. At each temperature, the morphology and structure of the Cu NPs were characterized by means of TEM, HRTEM, and ED using a Gatan OneView IS camera. On-line MS was recorded while real-time imaging under reaction conditions to monitor the changes in the gas phase.

In situ DRIFTS

In situ DRIFTS experiment was carried out on a Thermo Fisher Nicolet iS50 Fourier Transform Infrared Spectrometer equipped with a Harrick diffuse reflectance cell. After loading of a copper sample (mixed with inert SiO_2 to alter its color for enhanced signal), Ar gas (30 ml/min) was then passed through the reactor for 1 hour to eliminate adsorbed water molecules on the catalyst surface. Subsequently, the temperature was raised from room temperature to 200 °C. A background signal was recorded for later subtraction from the collected spectra. Following the removal of Ar, 10%C_2H_4 in Ar (30 ml/min) was introduced into the reactor for 45 minutes, with in situ DRIFTS spectra being recorded every 15 minutes under the applied condition. 0.25%O_2/Ar (10 ml/min) was then introduced into the ethylene flow (20 ml/min) at 200 °C, and IR spectra were captured every 15 minutes over a 45-minute period. The temperature was gradually increased in steps to 500 °C, with intervals of 50 °C, and in situ DRIFTS spectra were recorded at each temperature.

Image analysis

ImageJ software was utilized for image difference analysis, as illustrated in Fig. 1, with procedures detailed in our previous study[17]. Furthermore, ImageJ was utilized to create Movies from TEM images recorded during in situ TEM experiments. Radial profiles of SAED patterns were derived using the ImageJ plugin "Radial Profile Angle".

DFT calculations

DFT simulations were performed at the PBE level[61]. with the Quantum ESPRESSO package[62]. using pseudopotentials from the PSLibrary[63]. A plane wave basis with a kinetic energy cutoff of 35 Ry (350 Ry) was used to expand the electronic wavefunctions (charge density). Metallic surfaces were modeled as four-layer (4 × 4) (111) terminated surfaces using a (3 × 3 × 1) k-point mesh employed along with Marzari-Vanderbilt smearing using a smearing parameter of 0.02 Ry[64]. Oxide surfaces were modeled as four-layer (4 × 2) (110) terminated surfaces using a (3 × 3 × 1) k-point mesh employed along with Marzari-Vanderbilt smearing using a smearing parameter of 0.02 Ry. In all cases slabs were separated from their periodic images by ca. 15 Å of vacuum. Partially reduced structures were obtained by reducing the surface oxygen coverage to 1/8 ML; the effect of removing subsurface oxygen was also studied by removing the first, and then the second subsurface oxygen layer while maintaining 1/8 ML adsorbed oxygen. Transition states were located using the climbing image nudged elastic band method[65], where minimum energy paths were discretized into 8 images with a single transition state. The forces were relaxed until the force on the climbing image dropped below 0.05 eV/Å.

Data availability

The data that support the findings of this study are included in the published article and its Supplementary Information files. These data are also available from the corresponding authors upon request.

References

1. Chao, H.-Y. et al. In situ and emerging Transmission Electron Microscopy for catalysis research. *Chem. Rev.* **123**, 8347–8394 (2023).
2. Pu, Y., He, B., Niu, Y., Liu, X. & Zhang, B. Chemical Electron Microscopy (CEM) for heterogeneous catalysis at nano: recent progress and challenges. *Research* **6**, 0043 (2023).
3. Alcorn, F. M., Jain, P. K. & van der Veen, R. M. Time-resolved transmission electron microscopy for nanoscale chemical dynamics. *Nat. Rev. Chem.* **7**, 256–272 (2023).
4. He, B., Zhang, Y., Liu, X. & Chen, L. In-situ transmission electron microscope techniques for heterogeneous catalysis. *ChemCatChem* **12**, 1853–1872 (2020).
5. Shen, B. et al. A single-molecule van der Waals compass. *Nature* **592**, 541–544 (2021).
6. Willinger, M. G. et al. A case of strong metal–support interactions: combining advanced microscopy and model systems to elucidate the atomic structure of interfaces. *Angew. Chem. Int. Ed.* **53**, 5998–6001 (2014).
7. Ruska, E. Beitrag zur übermikroskopischen Abbildung bei höheren Drucken. *Kolloid-Z.* **100**, 212–219 (1942).
8. Gai, P. L. & Boyes, E. D. In-situ environmental (scanning) transmission electron microscopy of catalysts at the atomic level. *J. Phys.: Conf. Ser.* **522**, 012002 (2014).

9. Wagner, J. B., Cavalca, F., Damsgaard, C. D., Duchstein, L. D. L. & Hansen, T. W. Exploring the environmental transmission electron microscope. *Micron* **43**, 1169–1175 (2012).
10. Sharma, R. An environmental transmission electron microscope for in situ synthesis and characterization of nanomaterials. *J. Mater. Res.* **20**, 1695–1707 (2005).
11. Boyes, E. D. & Gai, P. L. Environmental high resolution electron microscopy and applications to chemical science. *Ultramicroscopy* **67**, 219–232 (1997).
12. Huang, X. et al. Visualizing structural and chemical transformations of an industrial $Cu/ZnO/Al_2O_3$ pre-catalyst during activation and CO_2 reduction. *ChemCatChem* **14**, e202201280 (2022).
13. Huang, X. et al. Phase coexistence and structural dynamics of redox metal catalysts revealed by *Operando* TEM. *Adv. Mater.* **33**, 2101772 (2021).
14. Frey, H., Beck, A., Huang, X., van Bokhoven, J. A. & Willinger, M. G. Dynamic interplay between metal nanoparticles and oxide support under redox conditions. *Science* **376**, 982–987 (2022).
15. Yuan, W. et al. In situ manipulation of the active Au-TiO_2 interface with atomic precision during CO oxidation. *Science* **371**, 517–521 (2021).
16. Beck, A. et al. The dynamics of overlayer formation on catalyst nanoparticles and strong metal-support interaction. *Nat. Commun.* **11**, 3220 (2020).
17. Yue, S. et al. Redox dynamics and surface structures of an active palladium catalyst during methane oxidation. *Nat. Commun.* **15**, 4678 (2024).
18. Zhang, L. et al. In situ visualization and mechanistic understandings on facet-dependent atomic redispersion of Platinum on CeO2. *Nano Lett.* **23**, 11999–12005 (2023).
19. Luo, L. et al. Real-time atomic-scale visualization of reversible copper surface activation during the CO oxidation reaction. *Angew. Chem. Int. Ed.* **59**, 2505–2509 (2020).
20. Zhang, X. et al. Reversible loss of core–shell structure for Ni–Au bimetallic nanoparticles during CO2 hydrogenation. *Nat. Catal.* **3**, 411–417 (2020).
21. Liu, X. et al. Atomically resolved transition pathways of iron Redox. *J. Am. Chem. Soc.* **146**, 17487–17494 (2024).
22. Niu, Y. et al. Patterning the consecutive Pd_3 to Pd_1 on Pd_2Ga surface via temperature-promoted reactive metal-support interaction. *Sci. Adv.* **8**, eabq5751 (2022).
23. Vendelbo, S. B. et al. Visualization of oscillatory behaviour of Pt nanoparticles catalysing CO oxidation. *Nat. Mater.* **13**, 884–890 (2014).
24. Xiong, H. et al. In situ imaging of the sorption-induced subcell topological flexibility of a rigid zeolite framework. *Science* **376**, 491–496 (2022).
25. Hansen, P. L. et al. Atom-resolved imaging of dynamic shape changes in supported copper nanocrystals. *Science* **295**, 2053–2055 (2002).
26. Plodinec, M., Nerl, H. C., Girgsdies, F., Schlögl, R. & Lunkenbein, T. Insights into chemical dynamics and their impact on the reactivity of Pt nanoparticles during CO oxidation by *Operando* TEM. *ACS Catal.* **10**, 3183–3193 (2020).
27. Ghosh, T. et al. Periodic structural changes in Pd nanoparticles during oscillatory CO oxidation reaction. *Nat. Commun.* **13**, 6176 (2022).
28. Tauster, S. J., Fung, S. C. & Garten, R. L. Strong metal-support interactions. Group 8 noble metals supported on titanium dioxide. *J. Am. Chem. Soc.* **100**, 170–175 (1978).
29. Cao, J. et al. In situ observation of oscillatory redox dynamics of copper. *Nat. Commun.* **11**, 3554 (2020).
30. Sun, X. et al. Surface-reaction induced structural oscillations in the subsurface. *Nat. Commun.* **11**, 305 (2020).
31. Sun, X. et al. Dislocation-induced stop-and-go kinetics of interfacial transformations. *Nature* **607**, 708–713 (2022).
32. LaGrow, A. P., Ward, M. R., Lloyd, D. C., Gai, P. L. & Boyes, E. D. Visualizing the Cu/Cu_2O interface transition in nanoparticles with environmental scanning Transmission Electron Microscopy. *J. Am. Chem. Soc.* **139**, 179–185 (2017).
33. Santra, A. K., Cowell, J. J. & Lambert, R. M. Ultra-selective epoxidation of styrene on pure Cu{111} and the effects of Cs promotion. *Catal. Lett.* **67**, 87–91 (2000).
34. Cowell, J. J. et al. Bonding and reactivity of styrene on Cu(110): heterogeneous alkene epoxidation without the use of silver. *Surf. Sci.* **437**, 1–8 (1999).
35. Cropley, R. L. et al. Copper is highly effective for the epoxidation of a "difficult" alkene, whereas silver is not. *Surf. Sci.* **578**, L85–L88 (2005).
36. Kokalj, A., Gava, P., de Gironcoli, S. & Baroni, S. What determines the catalyst's selectivity in the ethylene epoxidation reaction. *J. Catal.* **254**, 304–309 (2008).
37. Greiner, M. T., Jones, T. E., Klyushin, A., Knop-Gericke, A. & Schlögl, R. Ethylene epoxidation at the phase transition of copper oxides. *J. Am. Chem. Soc.* **139**, 11825–11832 (2017).
38. Farra, R. et al. Multi-scale Red-Ox dynamics of active metal catalysts revealed by a combination of in situ scanning and Transmission Electron Microscopy. *Microsc. Microanal.* **23**, 922–923 (2017).
39. Tang, M. et al. Oscillatory active state of a Pd nanocatalyst identified by in situ capture of the instantaneous structure–activity change at the atomic scale. *J. Am. Chem. Soc.* **146**, 18341–18349 (2024).
40. Reuter, K. & Scheffler, M. First-principles atomistic thermodynamics for oxidation catalysis: surface phase diagrams and catalytically interesting regions. *Phys. Rev. Lett.* **90**, 046103 (2003).
41. Rogal, J., Reuter, K. & Scheffler, M. CO oxidation at Pd(100): A first-principles constrained thermodynamics study. *Phys. Rev. B* **75**, 205433 (2007).
42. Greiner, M. T. et al. The oxidation of copper catalysts during ethylene epoxidation. *Phys. Chem. Chem. Phys.* **17**, 25073–25089 (2015).
43. Railsback, J. G., Johnston-Peck, A. C., Wang, J. & Tracy, J. B. Size-dependent nanoscale Kirkendall effect during the oxidation of Nickel nanoparticles. *ACS Nano* **4**, 1913–1920 (2010).
44. Rice, K. P., Paterson, A. S. & Stoykovich, M. P. Nanoscale Kirkendall effect and oxidation kinetics in copper nanocrystals characterized by real-time, in situ optical Spectroscopy. *Part. Part. Syst. Charact.* **32**, 373–380 (2015).
45. Yue, S. et al. Structural and chemical transformations of CuZn alloy nanoparticles under reactive redox atmospheres: An in situ TEM study. *Nano Res.* **17**, 6265–6273 (2024).
46. Böcklein, S. et al. Detection and quantification of steady-state ethylene oxide formation over an Ag(111) single crystal. *J. Catal.* **299**, 129–136 (2013).
47. Griffiths, J. F. & Perche, A. The spontaneous decomposition, oxidation and ignition of ethylene oxide under rapid compression. *Symp. (Int.) Combust.* **18**, 893–901 (1981).
48. Crocco, L., Glassman, I. & Smith, I. E. Kinetics and mechanism of ethylene oxide decomposition at high temperatures. *J. Chem. Phys.* **31**, 506–510 (1959).
49. White, A. G. & Joses, E. Ignition of acetaldehyde-air and acetaldehyde-oxygen mixtures. *J. Soc. Chem. Ind.* **69**, 206–209 (1950).
50. Lebron, G. B. & Tan, T. L. Integrated Band Intensities of Ethylene ($^{12}C_2H_4$) by Fourier Transform Infrared Spectroscopy. *Int. J. Spectrosc.* **2012**, 474639 (2012).
51. D'Oliveira, M. R., Rabelo, J., Veiga, A. G., Chagas, C. A. & Schmal, M. In Situ DRIFTS investigation of ethylene oxidation on Ag and Ag/Cu on reduced graphene oxide. *Catal. Lett.* **150**, 3036–3048 (2020).

52. Amorim de Carvalho, M. C. N., Passos, F. B. & Schmal, M. Study of the active phase of silver catalysts for ethylene epoxidation. *J. Catal.* **248**, 124–129 (2007).
53. Bulushev, D. A., Paukshtis, E. A., Nogin, Y. N. & Bal'zhinimaev, B. S. Transient response and infrared studies of ethylene oxide reactions on silver catalysts and supports. *Appl. Catal. A: Gen.* **123**, 301–322 (1995).
54. Torres, D., Lopez, N., Illas, F. & Lambert, R. M. Why copper is intrinsically more selective than silver in alkene epoxidation:Ethylene Oxidation on Cu(111) versus Ag(111). *J. Am. Chem. Soc.* **127**, 10774–10775 (2005).
55. Özbek, M. O. & van Santen, R. A. The mechanism of ethylene epoxidation catalysis. *Catal. Lett.* **143**, 131–141 (2013).
56. Linic, S. & Barteau, M. A. Formation of a stable surface oxametallacycle that produces ethylene oxide. *J. Am. Chem. Soc.* **124**, 310–317 (2002).
57. Chen, D., Kang, P.-L. & Liu, Z.-P. Active site of catalytic ethene epoxidation: machine-learning global pathway sampling rules out the metal sites. *ACS Catal.* **11**, 8317–8326 (2021).
58. Soon, A., Todorova, M., Delley, B. & Stampfl, C. Thermodynamic stability and structure of copper oxide surfaces: A first-principles investigation. *Phys. Rev. B* **75**, 125420 (2007).
59. Tan, Y. et al. Redox-driven surface generation of highly active Pd/PdO interface boosting low-temperature methane combustion. *Chin. J. Catal.* **60**, 242–252 (2024).
60. Zou, L., Li, J., Zakharov, D., Stach, E. A. & Zhou, G. In situ atomic-scale imaging of the metal/oxide interfacial transformation. *Nat. Commun.* **8**, 307 (2017).
61. Perdew, J. P., Burke, K. & Ernzerhof, M. Generalized gradient approximation made simple. *Phys. Rev. Lett.* **77**, 3865–3868 (1996).
62. Giannozzi, P. et al. QUANTUM ESPRESSO: a modular and open-source software project for quantum simulations of materials. *J. Phys.: Condens. Matter* **21**, 395502 (2009).
63. Dal Corso, A. Pseudopotentials periodic table: From H to Pu. *Comput. Mater. Sci.* **95**, 337–350 (2014).
64. Marzari, N., Vanderbilt, D., De Vita, A. & Payne, M. C. Thermal contraction and disordering of the Al(110) surface. *Phys. Rev. Lett.* **82**, 3296–3299 (1999).
65. Henkelman, G., Uberuaga, B. P. & Jónsson, H. A climbing image nudged elastic band method for finding saddle points and minimum energy paths. *J. Chem. Phys.* **113**, 9901–9904 (2000).

Acknowledgements

Prof. C. Copéret from ETH Zurich is acknowledged for the support of this research. X.H. thanks the 1000 Talent Youth Project, National Natural Science Foundation of China (22472027, 22421002), Fuzhou University (511027), Qingyuan Innovation Laboratory (00524006), and ETH Career Seed Grant (SEED–14 18-2) for the financial support.

Author contributions

X.H. conceived the idea, carried out the *operando* TEM experiments, and performed the data analysis and data visualization. T.J. conducted theoretical simulations. M.H. assisted with the MS measurement. W.Q.Y. carried out the in situ DRIFTS experiment. W.Q.Y., S.N.Y., M.H.Y., P.P.L., L.Z., and W.J.X. contributed to the data analysis and data visualization. X.H., M.W., and T.J. wrote and edited the manuscript.

Competing interests

The authors declare no competing interests.

Additional information

Supplementary information The online version contains supplementary material available at https://doi.org/10.1038/s41467-025-57418-0.

Correspondence and requests for materials should be addressed to Travis Jones, Marc Willinger or Xing Huang.

Peer review information *Nature Communications* thanks Guangwen Zhou and the other, anonymous, reviewer(s) for their contribution to the peer review of this work. A peer review file is available.